Spin-Wave Interference in Microscopic Rings

J. Podbielski,* F. Giesen, and D. Grundler†

Institut für Angewandte Physik und Mikrostrukturforschungszentrum, Universität Hamburg, Jungiusstrasse 11, 20355 Hamburg, Germany

(Received 4 November 2005; published 27 April 2006)

We have studied the spin excitations of ferromagnetic rings and observed a distinct series of quantized modes in the vortex state. We attribute them to spin waves that circulate around the ring and interfere constructively. They form azimuthal eigenmodes of a magnetic ring resonator which we resolve up to the fourth order. The eigenfrequencies are calculated semianalytically and classified as a function of magnetic field by a quantization rule which takes into account a periodic boundary condition. Strikingly each mode exists only below a characteristic field.

DOI: 10.1103/PhysRevLett.96.167207 PACS numbers: 75.40.Gb, 75.75.+a, 76.50.+g

When the lateral dimensions of a microstructured ferromagnet are on the order of the spin-wave wavelength λ, the geometrical boundaries impose a quantization condition for excitations. This has been found experimentally for straight micromagnets such as wires or rectangular prisms [1–7]. Curved ferromagnetic devices have recently attracted considerable interest due to flux-closure states with vanishingly small stray field and the circular symmetry of magnetization [8,9]. Quantization phenomena for disks in the vortex state [10] are, however, complex: due to the presence of a vortex core radial and azimuthal nodes do not, in general, represent good quantum numbers. A clear separation in radial and azimuthal spin waves [11–14] is not always possible [10] and the calculation of the eigenmodes and eigenfrequencies is involved [15–17].

We have investigated nanostructured permalloy ($Ni_{80}Fe_{20}$) rings which are in the vortex state [8] and where the core is removed. We observe quantized azimuthal spin waves up to the fourth order. They appear in a stepwise manner with overall negative magnetic field dispersion when we increase the applied magnetic field H. Our semianalytical calculations show that the steps originate from backward volume magnetostatic waves [18] which interfere around the ring. For each eigenmode an upper critical field exists. With increasing H in the vortex state, a further mode appears with positive magnetic field dispersion showing *no* discrete steps. This behavior is due to a localization phenomenon. Our observation that for propagating spin waves a ring acts as a ring resonator with quantized azimuthal modes is stimulating for both further fundamental spin dynamics research [19] and magneto-logical applications [20].

The fabrication of rings on the signal line of coplanar waveguides (CPWs) using electron beam lithography and lift-off processing has been described elsewhere [21,22]. We investigated three arrays which consisted of permalloy rings with similar width $w \approx 600$ nm and outer diameter $2R \approx 2000$ nm but had (i) different thickness t, (ii) different ring-to-ring separations and (iii) a different number of rings. They all displayed the same characteristics in the vortex state on which we report. Only the absolute values of the measured spin-wave eigenfrequencies varied (as expected, e.g., from the different thickness). We focus here on the data of one sample. It consisted of 750 nominally identical rings with $2R = 1950(\pm 30)$ nm, $w = 600(\pm 30)$ nm, and $t = 30(\pm 6)$ nm. The geometric parameters were determined by atomic force microscopy (AFM). The ring-to-ring separation of 2 μm excluded dipolar interaction [23]. Transmission spectra are measured at room temperature by means of a vector network analyzer connected to the CPW. The sinusoidal output signal of power 1 mW causes a high-frequency magnetic field H_{rf} surrounding the central conductor of the CPW and acting mainly in the plane of the rings. A static external magnetic field $\mu_0 H$ is applied parallel to the CPW and orthogonal to H_{rf}. Following Refs. [10,14] H_{rf} leads to a spatially inhomogeneous torque $\vec{m} \times \vec{H}_{\mathrm{rf}}$ in the vortex state [cf. Figure 3(a)]; i.e., spin-wave excitation is inhomogeneous.

In Fig. 1 we summarize a series of absorption spectra taken at different in-plane fields $\mu_0 H$ ranging from -60 to $+60$ mT. At each field the spectrum was recorded *after* applying a saturation field of $+90$ mT. The rings exhibit the typical reversal behavior with two irreversible switching processes [23,24]: for $\mu_0 H \geq \mu_0 H_1^{\mathrm{sw}} = -2$ mT the rings are in the onion state. Lowering H below H_1^{sw} makes the rings switch to the vortex state. The absorption characteristics change significantly. The vortex configuration is stable down to $\mu_0 H_2^{\mathrm{sw}} = -18$ mT. For $H \leq H_2^{\mathrm{sw}}$ rings form the reversed onion state. The three separate regimes of dynamic response have already been reported for 250 nm wide rings [21]. Modes A and B, which are observed at high field in the *onion* state (see labels in Fig. 1), have already been explained by localized spin-wave excitations [21–23]. Mode A resides in ring segments where the external field is oriented tangentially to the ring, and mode B in domain walls. These localized modes at high field will not be discussed.

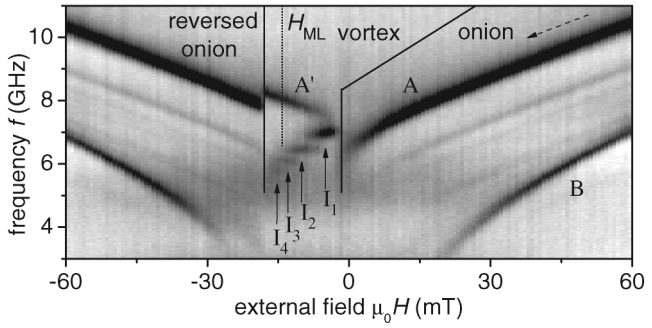

FIG. 1. Gray-scale plot of absorption spectra taken at successively decreased magnetic field (cf. dashed arrow) after saturation at $\mu_0 H = +90$ mT (onion state). Dark represents strong absorption. In the onion state modes A and B are detected consistent with Ref. [21]. In the vortex state discrete spin-wave eigenfrequencies I_1, I_2, I_3, I_4 (see labels) and A′ are resolved (cf. also Fig. 2). Black solid vertical lines indicate switching fields.

The intriguing novel observation in this work is the stepwise behavior in the vortex state (labeled by I_n with $n = 1, 2, 3, 4$). Here, spin-wave eigenfrequencies are discrete and form plateaus I_n which are found to be slightly magnetic field dependent. Clear frequency gaps of $\cong$ 500 MHz are resolved between the steps I_n. This interesting behavior is best seen in the minor loop of Fig. 2. For this, we have first saturated the rings at +90 mT and second applied $\mu_0 H = -14$ mT (cf. H_{ML} in Fig. 1) thus generating the vortex state. The regime of the vortex state can be identified easily: the spin-wave modes show a mirror symmetry with respect to $H = 0$ as argued in Ref. [21]. For $H = 0$ only mode I_1 is resolved at frequency $f = 7.04$ GHz. Each of the spin-wave excitations is detected within a characteristic field interval. The onset fields of modes I_n with $n = 2$, 3, and 4 are 4, 8, and 9 mT,

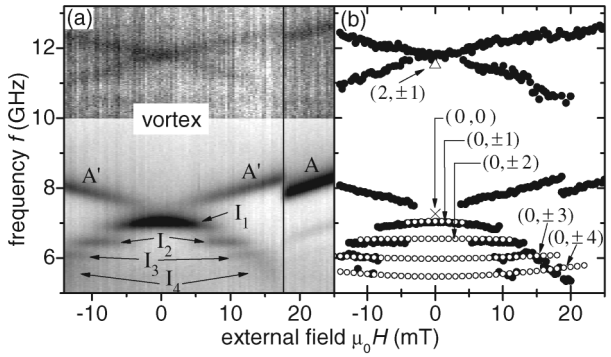

FIG. 2. (a) Gray-scale plot of spectra taken in the minor loop starting at −14 mT. Dark represents strong absorption. The contrast for 10 GHz $\leq f \leq$ 13.2 GHz is increased. (b) Full symbols are eigenfrequencies extracted from the individual absorption spectra. Open circles refer to the quantized modes calculated via Eq. (1). Numbers in brackets label the modes (m, n) from the semianalytical calculations.

respectively. The modes exist up to a critical field $H_{c,n}$: we find $\mu_0 H_{c,1} = 9$ mT for mode I_1, $\mu_0 H_{c,2} = 13$ mT and $\mu_0 H_{c,3} \approx 15$ mT. The critical field increases with increasing index n. At the same time the eigenfrequency decreases. The mode which is labeled by A′ in Figs. 1 and 2 is not resolved for -4 mT $< \mu_0 H < +4$ mT and shows no discrete steps. At high frequency we detect two additional modes of low signal strength which cross at 11.8 GHz in the remanent vortex state.

For the discussion let us first describe the details of our calculations. To recalculate the spin dynamics of rings we make use of the circular magnetization configuration as shown in Fig. 3(a). We adopt the notation from Ref. [10] and index the spin waves by the integer number of nodal lines m and n along the radial $\vec{e}_r$ and azimuthal $\vec{e}_\phi$ directions, respectively. The total wave vector K can then be decomposed by $K^2 = k_r^2 + k_\phi^2$, defined in Fig. 3(b). In radial direction due to the geometric ring borders a quantization condition is anticipated for k_r which is very similar to the one of a longitudinally magnetized wire [1,6,7]. This leads to discrete values $k_r = k_{mr}$. Important for this work is the azimuthal component k_ϕ which is parallel to the ring's magnetization and represents a backward volume magnetostatic wave (BVMSW). Here we argue that a quantization for the ring's azimuthal mode arises if

$$n 2\pi = \oint k_\phi(f, H_{\text{int}}(\phi)) r d\phi \tag{1}$$

is fulfilled, where r is the radius of the integration path and H_{int} the internal field, which includes the external, demagnetizing and effective exchange field. We will show later that for $H \neq 0$, H_{int} varies characteristically along ϕ. Then, the wave vector $k_\phi(\phi) = k_\phi(f, H_{\text{int}}(\phi))$ changes with ϕ through the variation of H_{int}. Equation (1) is the condition for constructive interference and ensures that a spin wave exhibits the same phase after propagating around the ring. In the following we outline how we recalculate the eigenfrequencies f_n using the quantization condition Eq. (1) and how we consider the finite external field H.

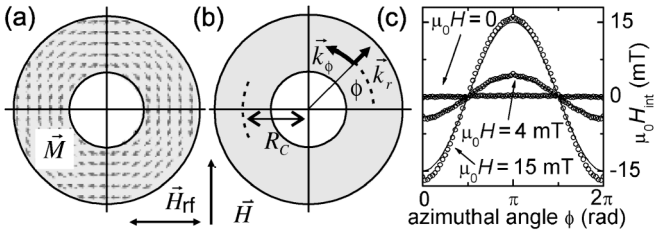

FIG. 3. (a) Symmetry of the experiment: $\vec{H}_{rf}$ and the external field $\vec{H}$ are orthogonal. Small arrows indicate the local magnetization $\vec{m}$ in the ring's vortex state. (b) Definition of parameters. (c) Spatial profile of the internal field H_{int} as a function of ϕ. $H \neq 0$ leads to a spatially oscillating field H_{int}, calculated by micromagnetic simulations [28] (open symbols) and modeled by $H_{\text{int}} = -H \cos\phi$ (solid line).

If we neglect the exchange energy in the remanent vortex state the ring is mathematically equivalent to a longitudinally magnetized wire which has no demagnetization field at the front and back end and which exhibits periodic boundary conditions along the long axis. Considering these characteristics one can use the dispersion relations $f(K, H_{\mathrm{int}})$ of Ref. [6] to calculate spin-wave excitations for a longitudinally magnetized wire forming a ring. The important difference to the straight wire occurs if one applies a magnetic field H to the ring: H_{int} becomes a spatially oscillating function. To keep the analysis simple, we focus in the following on the azimuthal direction ϕ at $r = R_{\mathrm{C}}$ [compare Fig. 3(b)]. Open symbols in Fig. 3(c) refer to a micromagnetic simulation of the internal field [25]. As can be seen, the functional form $H_{\mathrm{int}} = -H\cos\phi$ (solid lines) remodels the simulated internal field very well. This analytical form is a good approximation if at small field H deviations from the circular symmetry in Fig. 3(a) are negligible. The sign of the internal field is defined by the magnetization orientation: H_{int} is negative (positive) for an antiparallel (parallel) alignment of $\vec{M}$ and $\vec{H}$. Considering this $H_{\mathrm{int}} = -H\cos\phi$ in the formalism of the wire, we can then calculate the wave vector dispersion $f(k_{mr}, k_{\phi}, H_{\mathrm{int}})$ using Eqs. (7), (10), and (11) in Ref. [6] for different applied fields H [26]. Introducing position dependent wave vectors k_{ϕ} at $r = R_{\mathrm{C}}$ into Eq. (1) then defines the eigenfrequencies of the vortex state as outlined in detail later. The results of the semianalytical calculations are shown in Fig. 2(b) as open circles. The frequency gaps of about 500 MHz and the discrete spin-wave excitations I_n are reproduced very well. For the calculations we assumed $2R = 1920$ nm, $w = 630$ nm and $t = 26$ nm in excellent agreement with the AFM measurements. For the gyromagnetic ratio we took $\gamma = 28\ \frac{\mathrm{GHz}}{\mathrm{T}}$. The saturation magnetization $\mu_0 M_S = 1120$ mT was determined by ferromagnetic resonance measured on a reference film prepared in the same evaporation process. The good agreement between calculations and experiment in Fig. 2(b) already demonstrates that, in contrast to a disk [11,13], which is a topographically simply connected object, in rings the separation into azimuthal and radial modes is stringent. BVSMW's are guided around the ring and interfere.

To discuss the quantization phenomenon in detail let us refer to Fig. 4. Again it is instructive to start with $H = 0$ where the internal field is zero everywhere and the dispersion of the BVSMW is not position dependent. This simplifying case is shown in Figs. 4(a) and 4(d) where we assume for the radial direction $m = 0$. The wave vectors consistent with Eq. (1) are constant around the ring and are given by $k_{n\phi} = n/R_{\mathrm{C}}$. For the line integral we assumed the central line with radius $R_{\mathrm{C}} = R - \frac{w}{2}$ [cf. Figure 3(b)]. The corresponding frequencies labeled by I_n exhibit the gaps of about 500 MHz. At finite fields the dispersion of the BVSMW is position dependent and we obtain a band of dispersions. The case for $\mu_0 H = 4$ mT is shown in

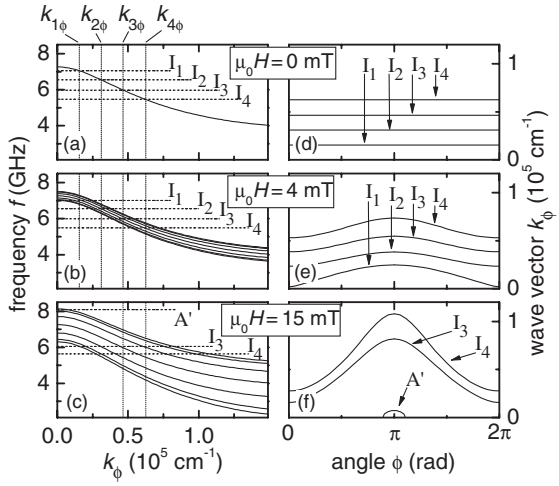

FIG. 4. (a)–(c) Wave vector dispersions for BVSMW's ($m = 0$) at azimuthal positions $\phi = \frac{i\pi}{6}$ with $i = 0, 1, 2, \ldots, 6$ and at external magnetic fields $\mu_0 H$ of 0 (a), 4 (b), and 15 mT (c). A dispersion band forms for $H \neq 0$. Horizontal lines indicate modes I_n ($n = 1, 2, 3, 4$) and mode A$'$. Vertical lines mark the specific wavelengths which fit n times into the ring at $H = 0$, i.e., $k_{n\phi} = n/R_{\mathrm{C}}$ on the top axis. In (d)–(e) the corresponding wave vectors are plotted against the azimuthal position ϕ reflecting the variation of H_{int}.

Fig. 4(b) where we depict dispersions for selected $\phi = \frac{i\pi}{6}$ with $i = 0, 1, 2, \ldots, 6$. The lower and upper "band edges" are given by the minimum and maximum internal field at $\phi = 0$ ($i = 0$) and $\phi = \pi$ ($i = 6$), respectively. The band broadens almost symmetrically around the dispersion of $H_{\mathrm{int}} = 0$. Graphically, wave vectors $k_{n\phi}(\phi)$ are found as intersections of the horizontal frequency lines I_n with the dispersions. The wave vectors which are consistent with Eq. (1) at 4 mT are depicted in Fig. 4(e). In particular, they now vary with ϕ. With higher magnetic field the position dependence of $k_{n\phi}(\phi)$ becomes more and more pronounced [Fig. 4(f)]. Because of the broadening of the dispersion band with increasing H the eigenfrequencies f_n become dependent on the applied field [cf. Figure 2(b)]. The overall variation however is small as the broadening is found to be rather symmetric.

The dispersion band at $\mu_0 H = 15$ mT in Fig. 4(c) explains why the spin-wave excitations are observed only below an upper critical field. The BVMSW must exist everywhere in the ring. For this the frequency lines I_n do first have to intersect *all* dispersion relations of the band and second have to fulfill Eq. (1). These criteria are true for I_3 and I_4 at $\mu_0 H = 15$ mT. Below $k_{3\phi}(\phi)$ in Fig. 4(f), however, no further wave vectors are found which are consistent with both requirements. BVMSW modes with $n = 1$ and $n = 2$ have vanished. The model thus correctly predicts upper critical fields $H_{\mathrm{c},n}$. They increase with increasing mode number n. The calculated modes shown as open symbols in Fig. 2(b) exist over the whole interval $[-H_{\mathrm{c},n}, +H_{\mathrm{c},n}]$, whereas we observe onset fields for $n \geq 2$

in the experiment. The calculations, however, do not include the specific excitation mechanism. The high-frequency field H_{rf} is homogeneous in the rings' plane. To excite BVMSW of high wave vectors $k_{n\phi}$ with $n \geq 2$ an inhomogeneous internal field H_{int} or a spatially inhomogeneous magnetization are needed. To generate this, we have to apply a finite field leading to the experimentally observed onset field. Following Refs. [14,27] we are not able to excite the uniform azimuthal mode $(m, n) = (0, 0)$ [cross at 7.26 GHz in Fig. 2(b)] with $k_\phi = 0$ due to both the symmetry of the vortex state and the orientation of H_{rf}.

To explain mode A′ in the vortex state we start from the measured frequency $f = 8.1$ GHz at $\mu_0 H = 15$ mT. In Fig. 4(c) this frequency lies at the upper edge of the dispersion band. $k_\phi(\phi)$ shown in Fig. 4(f) suggests that mode A′ is localized near $\phi = \pi$ since real values for the wave vector exist only for $\pi - \frac{\pi}{10} < \phi < \pi + \frac{\pi}{10}$. The corresponding localization length amounts to 420 nm. Because of the localization spin-wave interference around the ring is not possible and discrete steps are not expected in the magnetic field dispersion. This is in agreement with the experimental data. Mode A′ is similar to mode A in the onion state which was discussed in Refs. [21–23]. As the magnetization pattern and the internal field change between the vortex and the onion state this characteristic spin-wave excitation shifts to a different eigenfrequency. We note that mode A′ does not exist for -4 mT $< \mu_0 H <$ $+4$ mT in Fig. 2(b) and that the linear magnetic field dependence does not extrapolate to the uniform mode $(0, 0)$ at $H = 0$. This characteristic behavior needs further theoretical elucidation.

In the remaining paragraph we discuss the modes crossing at 11.8 GHz in Fig. 2(a). Here, our model suggests circulating (lower branch) and localized (upper branch) spin waves with two nodes, i.e., $m = 2$, in the radial direction. The calculated eigenfrequency of mode $(m, n) = (2, \pm 1)$ at $H = 0$ is shown as an open triangle in Fig. 2(b) and consistent with the data. We find that the BVMSW dispersions for $m = 2$ are flat (not shown), and that the calculated frequency gaps amount to only 100 MHz for increasing n and H. The low signal-to-noise ratio might have obscured the small gaps in the upper panel of Fig. 2(a). The width $w = 600$ nm used in this study thus was in a suitable regime to make the quantization of BVMSW's observable for $m = 0$.

In conclusion, we studied the spin dynamics of permalloy rings in the vortex state. Interfering spin waves formed the azimuthal eigenmodes. They were modeled by BVMSW's propagating along the ring and fulfilling a quantization condition. Consequently, a magnetic ring constitutes a microresonator for spin waves. The observations open new experimental perspectives for the spin-wave physics predicted in devices with topologically nontrivial magnetization profile [19,20].

The authors are grateful to D. Heitmann for his continuous support and thank C. Bayer for stimulating discussions. Financial support by the BMBF through Grant No. 13N8283 and by the DFG via SFB668 is acknowledged.

*Electronic address: jpodbiel@physnet.uni-hamburg.de
†Electronic address: grundler@ph.tum.de

[1] C. Mathieu *et al.*, Phys. Rev. Lett. **81**, 3968 (1998).
[2] J. Jorzick *et al.*, Phys. Rev. B **60**, 15 194 (1999).
[3] Y. Roussigne *et al.*, Phys. Rev. B **63**, 134429 (2001).
[4] J. Jorzick *et al.*, Phys. Rev. Lett. **88**, 047204 (2002); J. P. Park, P. Eames, D. M. Engebretson, J. Berezovsky, and P. A. Crowell, Phys. Rev. Lett. **89**, 277201 (2002).
[5] S. Tamaru *et al.*, J. Appl. Phys. **91**, 8034 (2002).
[6] K. Y. Guslienko, R. W. Chantrell, and A. N. Slavin, Phys. Rev. B **68**, 024422 (2003).
[7] K. Y. Guslienko, S. O. Demokritov, B. Hillebrands, and A. N. Slavin, Phys. Rev. B **66**, 132402 (2002).
[8] J. Rothman *et al.*, Phys. Rev. Lett. **86**, 1098 (2001).
[9] J. P. Park, P. Eames, D. M. Engebretson, J. Berezovsky, and P. A. Crowell, Phys. Rev. B **67**, 020403(R) (2003).
[10] J. P. Park and P. A. Crowell, Phys. Rev. Lett. **95**, 167201 (2005).
[11] M. Buess *et al.*, Phys. Rev. Lett. **93**, 077207 (2004).
[12] L. Giovannini *et al.*, Phys. Rev. B **70**, 172404 (2004).
[13] M. Buess *et al.*, Phys. Rev. B **71**, 104415 (2005).
[14] X. Zhu, Z. Liu, V. Metlushko, P. Grütter, and M. R. Freeman, Phys. Rev. B **71**, 180408(R) (2005).
[15] B. A. Ivanov and C. E. Zaspel, Phys. Rev. Lett. **94**, 027205 (2005); J. Appl. Phys. **95**, 7444 (2004); Appl. Phys. Lett. **81**, 1261 (2002).
[16] R. Zivieri and F. Nizzoli, Phys. Rev. B **71**, 014411 (2005).
[17] C. E. Zaspel, B. A. Ivanov, J. P. Park, and P. A. Crowell, Phys. Rev. B **72**, 024427 (2005).
[18] R. W. Damon and J. R. Eshbach, J. Phys. Chem. Solids **19**, 308 (1961).
[19] V. K. Dugaev, P. Bruno, B. Canals, and C. Lacroix, Phys. Rev. B **72**, 024456 (2005).
[20] R. Hertel, W. Wulfhekel, and J. Kirschner, Phys. Rev. Lett. **93**, 257202 (2004).
[21] F. Giesen *et al.*, Appl. Phys. Lett. **86**, 112510 (2005).
[22] F. Giesen *et al.*, J. Appl. Phys. **97**, 10A712 (2005).
[23] J. Podbielski *et al.*, Superlattices Microstruct. **37**, 341 (2005).
[24] H. Rolff *et al.*, J. Magn. Magn. Mater. **272–276**, 1623 (2004).
[25] We have used the OOMMF code to simulate the internal field of the ring and extracted the data at $r = R_{\mathrm{C}}$. The parameters in the simulation were: $D = 2000$ nm, $w = 600$ nm, $t = 30$ nm, $A = 13 \times 10^{-12}$ J/m, $\mu_0 M_s = 1120$ mT. The cell size was $4 \times 4 \times 30$ nm^3.
[26] We replace k_{mx} and k_{ny} in Ref. [6] by k_{mr} and $k_{n\phi}$, respectively.
[27] X. Zhu *et al.*, Appl. Phys. Lett. **86**, 262502 (2005).
[28] M. J. Donahue and D. G. Porter, *OOMMF User's Guide, Version 1.0* (1999).